# Comparison of Diesel Fuel and Hydrogenated Vegetable Oil Combustion in an Optical Engine by Means of Simultaneous Two-Colour Imaging and OH* Chemiluminescence

P. Dragomirov [1], J. Sauerhering[1], J. Hadler[2], H. Rottengruber[3], J. Schmidt[1], F. Beyrau*,[1]

[1] Institute of Fluid Dynamics and Thermodynamics, Otto von Guericke University of Magdeburg, Germany
[2] Institute of Automotive Expertise, Otto von Guericke University of Magdeburg, Germany
[3] Institute of Mobile Systems, Otto von Guericke University of Magdeburg, Germany

**Abstract**

The combustion behaviour of common Diesel fuel was compared with that of hydrated vegetable oil (HVO), a so called 2nd generation bio-fuel. Simultaneous two-colour imaging to determine soot temperatures and soot cloud densities expressed via the KL-factor, as well as OH* chemiluminescence detection were applied in an optically accessible diesel engine. The combustion analysis showed significant differences between the fuels. A larger area of early in-cylinder soot was observed in the case of HVO, in contrast to the measured lower soot engine emission from the opacimeter. The smoke opacity results correlate well with the lower average KL-factor for HVO. In general higher in-cylinder soot temperatures as well as considerably stronger OH* chemiluminescence have been detected during the combustion of HVO, which indicates better soot oxidation.

## Introduction

With rising concerns about limited resources and environmental pollution along with the establishment of the electromobility on the market, further development of compression ignition engines is highly desirable, in order to reduce fuel consumption as well as particulate- and $CO_2$-emissions. Regarding the latter, the use of new fuels, particularly bio fuels, is increasingly important. Even though alternative fuels are generally engineered to be similar to Diesel fuel, there are significant differences in their physical and chemical properties, which could lead to different combustion and exhaust emission characteristics. With this aim, the combustion behavior of two fuels, common Diesel fuel and hydrated vegetable oil, was studied.

## Single-cylinder test bed

In this work a single cylinder research engine (type AVL 5402) derived from a 2.0 litre, 4 cylinder engine was used. It has a centrally-positioned injector and 2 intake and 2 outlet valves. Further specifications of the optical engine are listed in Table 1.

**Table 1** Engine specifications

| | | |
|---|---|---|
| Max. speed | 3000 | $min^{-1}$ |
| Max. cylinder pressure | 80 | bar |
| Compression ratio | 13 | - |
| Engine cycle | 4 stroke | - |
| Stroke | 95.5 | mm |
| Bore | 81 | mm |

The original 2.0 litre engine was customised by AVL as follows to achieve optical accessibility to the combustion chamber. A 34 mm high and 30 mm thick silica glass ring or an optional metal ring can be mounted to the cylinder head via a metal holder. The serial production piston is replaced by an elongated piston consisting of a hollow piston rod and a piston top, see Figure 1. The hollow piston rod allows a 45° elliptical mirror to be positioned inside it. To avoid fouling of the engine's optical components the piston top runs oil-free.

The lowered position of the compression ring along with the 1.5 mm gap between the cylinder head and the piston is responsible for the relatively low compression ratio of 13.

The research engine is mounted on a compact single-cylinder test bed equipped with an electric drive unit, first order mass balance, oil and water as well as fuel conditioning units.

**Figure 1** Elongated piston and 45° mirror

An external supercharger is in place and piezoelectric pressure transducers are installed to indicate the cylinder as well as the intake pressure. In addition the research engine was equipped with a lambda sensor and an AVL 439 opacimeter to measure the smoke opacity.

In this work a common rail injection system was used with a solenoid driven injector. The injection system was operated by a free adjustable control unit ($FI^2$) and more detailed information is listed in Table 2.

**Table 2** Injection system specifications

| | |
|---|---|
| Fuel injection system | Common rail, Bosch |
| Pump | CP3, Bosch |
| Injector actuation | Solenoid, Bosch |
| Nozzle type | Seat hole |
| Nozzle hole number | 8 |
| Diameter of the orifice | 109 µm |
| Inclination angle of the orifice | 81.39° |

## Fuels and operating conditions

To contribute to the characterisation of alternative Diesel fuels, the bio-fuel, hydrogenated vegetable oil

* Corresponding author: frank.beyrau@ovgu.de

(HVO), was selected for combustion and comparative analysis with conventional Diesel fuel.

The indicated mean effective pressure (IMEP) and the centre of combustion (MBF 50 %) were set to approximately 3 bar and 10.5 °CA after top dead centre (TDC) to minimise the risk of damaging the glass components. An engine speed of 1500 $min^{-1}$ and a rail pressure of 1100 bar were selected. Additionally the research engine was super-charged with approximately 200 mbar.

The differences in the chemical properties of the fuels, e.g. the cetane number (round 75 and 51 respectively for HVO and Diesel fuel) and lower heating value, lead to noticeable deviations in their ignition delay and combustion in general. In order to keep the operating parameters (BMEP and MBF50%) constant the injection timings, start of energising (SOE) and energising time (ET), of the fuels needed to be adjusted, see Table 3.

**Table 3** Injection settings for the investigated fuels

| Fuel [-] | SOE pilot [° CA] | ET pilot [µs] | SOE main [° CA] | ET main [µs] |
|---|---|---|---|---|
| Diesel | -13.3 | 180 | 2.2 | 240 |
| HVO | -7.6 | 140 | 2.2 | 285 |

**Set-up for simultaneous soot and OH* detection**

With the goal of analysing the soot formation and oxidation processes OH radicals and incandescent soot particles were detected. Due to the risk of window fouling and the challenge to keep combustion parameters stable for longer time it is advantageous to conduct the experiments in only a few cycles. Therefore the following high speed measurement systems were applied.

One colour CMOS high speed camera (LaVision Imager ProX 4M) was used to visualise the natural soot luminosity within the visible range with a 105 mm Nikon lens. Second camera coupled with a high speed intensified relay optic system (IRO) and 100 mm LaVision UV lens was utilised to capture the OH* chemiluminescence. The light emissions from combustion were directed to both camera systems by a UV beam splitter, see transmission specifications in Figure 3 and experimental setup in Figure 2.

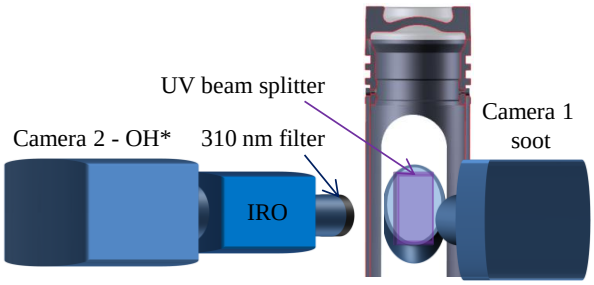


**Figure 2** Experimental set-up for Soot/OH detection

The OH radicals originating from the combustion of hydrocarbons are in an exited state (OH*) and emit energy in form of UV-light in order to return to their ground state. These emissions have a peak intensity at about 300 to 310 nm [1, 2] and [3] .

A band-pass filter at 310 nm with a full width at half maximum of 10 nm was used during the visualisation of the OH* chemiluminescence to reject emissions from other radicals and the thermal radiation from the soot particles.

The combustion visualisation was conducted at a frame rate of 9 kHz, which corresponds to 1 °CA at an engine speed of 1500 $min^{-1}$. The trigger point for the camera was set to 5 °CA before TDC and the combustion was investigated up to 55 °CA after TDC. Based on the selected recording frequency the camera resolution was limited to 576 x 580.

**Image post processing**

Prior to the image acquisition dark image subtraction was performed. Due to the lens-type formed ω-cavity of the piston bowl, the combustion images are distorted. Additionally the image distortion is a function of the crank angle position.

To account for these aberrations a correction routine was developed. The cameras were focused at a calibration plate positioned at 10 °CA after TDC. Afterwards calibration images at different piston positions were taken. The generated calibration images were then de-warped using the commercial software DaVis, hereby the necessary correction functions were created. Due to the little movement of the piston near TDC all combustion images acquired near TDC are corrected with calibration based on 10 °CA after TDC.

To avoid background reflections affecting the combustion analysis all pixels with a lower pixel count value than a predefined threshold, 25% of the image's average intensity, are reset to zero. For each colour the threshold is calculated separately and if the pixel value for one of the colours is lower than the estimated threshold, all colours are reset to zero.

Prior to the analysis of the soot luminosity images the combustion images were smoothed in order to reduce the effects of shot to shot noise and other random fluctuations in the measured count values.

**Two-colour imaging**

The colour flame images can also be used to obtain information about the temperature and optical thickness of the soot clouds by applying the two-colour imaging technique.

The two-colour method is a well-established line of sight technique for analysis of diffusion flames and was first-introduced by Hottel and Broughton [4]. Individual incandescent soot particles as well as thick uniform soot clouds could be treated as black bodies, where the radiation of black bodies can be expressed by Planck's law , where $C_1$ and $C_2$ are the first and second radiation constants:

$$E_{\lambda,b}(T,\lambda) = \frac{C_1}{\lambda^5\left[e^{C_2/\lambda T}-1\right]} \qquad (1)$$

However less dense clouds would have a lower

emissive power and therefore cannot be assumed to behave as black bodies. This relation can be expressed by the following equation:

$$E_\lambda(T,\lambda) = \varepsilon_\lambda E_{\lambda,T}(T,\lambda) \quad (2)$$

Hottel and Broughton's [4] correlation for the monochromatic emissivity is a function of the optical thickness (L) of the soot cloud along the observation axis and the absorption coefficient (K), which represents the particle number density or the soot volume fraction:

$$\varepsilon_\lambda = 1 - e^{\frac{-KL}{\lambda^\alpha}} \quad (3)$$

The absorption coefficient (L) and the optical thickness (K) are usually reported as a product (KL) and this approach is used in this study. In equation 3 α is an empirical constant and according to Zhao and Ladommatos [5] the calculated temperatures are relatively insensitive to α for the visible range. A constant value of 1.39 was used as suggested by [5]. Recently, colour cameras are frequently used for two-colour imaging (e.g. [6] and [7]). This is due to their advantages in comparison to a standard two camera system, such as the reduced number of cameras and no requirement for camera mapping on the pixel level. The pixels of the CMOS colour camera used in this study are equipped with broadband red, green and blue filters, which selectively transmit light in the visible range (Fig. 4) and are arranged in the Bayer-pattern. Broadband filters can be accounted for as already proven by [8] and [7] and thereby the use of effective wave lengths is no longer necessary.

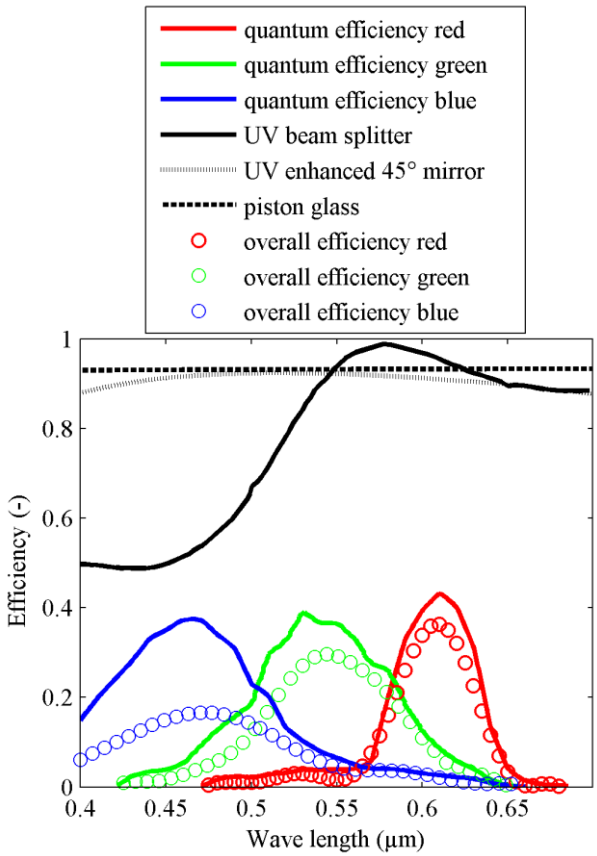


**Figure 3** Efficiency of the optical components

For the case of the colour camera the relation between the measured intensity by the camera and the radiative power of the soot clouds can be expressed by equation 4 following the approach of [8].

$$I_i = \int_{t_1}^{t_2}\int_{\lambda_1}^{\lambda_2} s_i \gamma_i \varepsilon_\lambda E_{\lambda,b}\, d\,\lambda dt \quad (4)$$

The measured pixel count $I_i$, where "$i$" indicates the colour channel, is a function of thermal radiation $E_{\lambda,b}$ and emissivity of the soot cloud $\varepsilon_\lambda$.The overall efficiency of the whole system $\gamma_i$ accounts for all known values: the camera's quantum efficiency, the transmittance efficiency of the UV beam splitter and the piston glass as well as for the reflective properties of the UV enhanced 45° mirror, see image Figure 3. In equation 4 $s_i$ is a unknown conversion constant, with which the incident light is being converted to pixel counts.

To obtain the unknown variables $s_i$ the system was calibrated for two-colour imaging using a high temperature Mikron M335 black body calibration source. For the calibration process the same optical components as in the real experiments were used, aligned at roughly the same distance to each other as in the experimental setup shown in Figure 2.

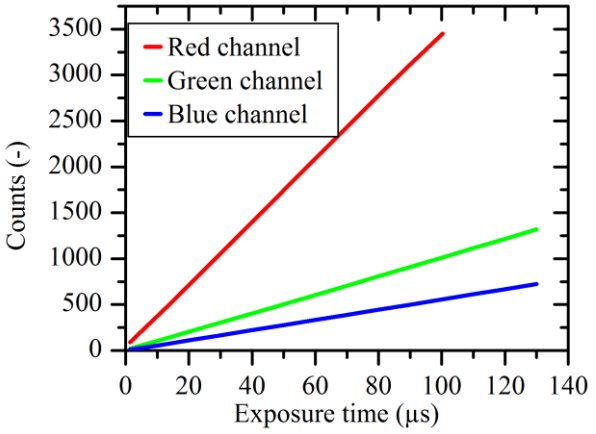


**Figure 4** Linearity of the colour channels

Average images containing 20 images were taken at temperatures ranging between 1273 and 1773 K, and a 71 by 71 pixel window with a spatially uniform intensity was extracted for the calibration process. All three colour channels exhibited linear behaviour with increasing incident light intensity, see Figure 4. Using equation 4 the conversion constants for the three colour channels could be estimated, where the emissivity of the black body source is equal to 1.

The calculation of the soot temperature and KL-factor is only possible taking some assumptions, like a uniform distribution along the soot clouds into account. The use of Hotel and Broughton's correlation for the emissivity of the soot also brings uncertainties, which were already discussed in the literature by [5]. The combustion images also depend on fouling of the glass

piston surface. However no deterioration of the quality of the combustion image during the cycles selected for analysis could be observed.

**Results and discussion**

The average values of 10 cycles for both investigated fuels are discussed in this section. The area of the images containing soot calculated from the combustion images are shown in Figure 5 as a function of the crank angle and normalised to the highest value for the Diesel fuel. There is a delay in the soot formation process of HVO noticeable comparing the slope of the curves in Figure 5. A nearly 20% larger soot area could be detected in the case of HVO for the most parts of the combustion, which might indicate that during the combustion of HVO more soot matter is formed and therefore may remain at the end. In the literature [9], [10] and [11] is also reported that the combustion of fuels with higher cetane number like HVO have soot luminosity with stronger intensity and larger areas containing soot luminosity.

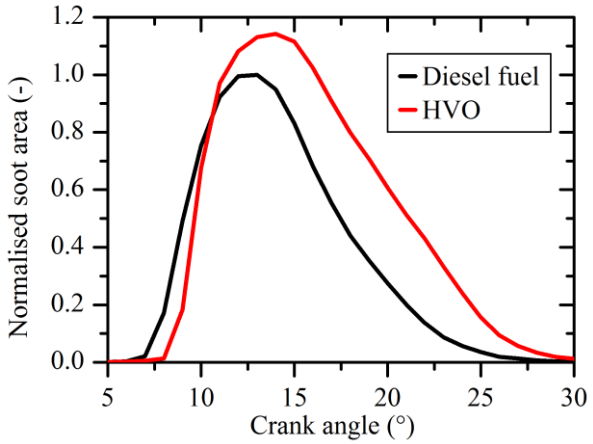


**Figure 5** Normalised soot area

However the smoke opacity measurements indicate twice the smoke emission in the case of the Diesel fuel, see Figure 6, and thereby contradicts the qualitative result obtained by the detection of the natural soot luminosity.

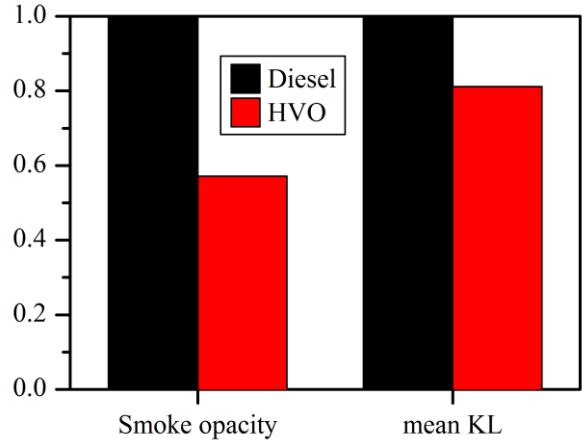


**Figure 6** Normalised smoke opacities and mean KL values

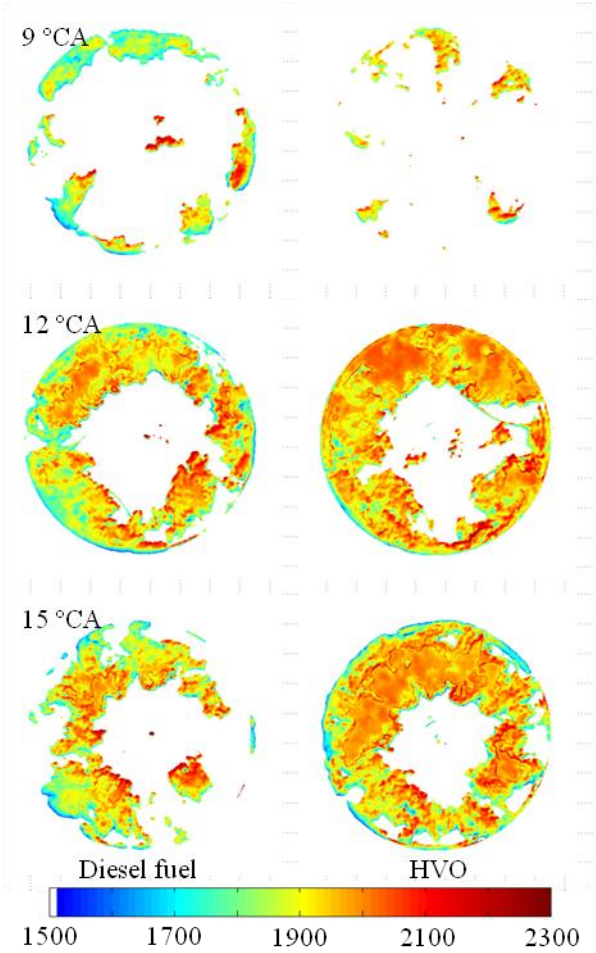


**Figure 7** Soot temperature distributions in degrees K at chosen crank angle positions

The two-colour temperature measurements were used to investigate this contradiction. Representative temperature fields for the two fuels are illustrated for three crank angle positions, see Figure 7.

In Figure 7 at 9 °CA after TDC a smaller soot area can be observed for HVO as already illustrated by Figure 5. Furthermore HVO has a more homogenous temperature field in comparison to the Diesel fuel, which exhibits large soot areas with noticeably lower temperatures as well as local hot spots.

At 12 °CA after TDC the HVO combustion has already reached larger soot areas than Diesel fuel, but the soot temperatures are higher and feature a more uniform distribution. This trend can be also observed in later crank angles as for example 15 °CA after TDC, see Figure 7.

The averaged calculated soot temperatures and the standard deviations between the 10 cycles are illustrated in Figure 8. The mean soot temperatures depict the same trend, in terms of higher soot temperatures for HVO, presented by the single temperature fields in Figure 7. The differences between the fuels are bigger at the early stages of the combustion process probably due to superior ignition properties. Even though the soot temperatures are not the same as the gas temperatures, the higher soot temperatures in the case of HVO may

indicate higher combustion temperatures in general. Moreover the cyclic fluctuations of HVO's soot temperatures are smaller than diesel's suggesting more stable combustion behaviour, which could also be confirmed by the pressure traces. The standard deviations of MBF50% and of IMEP are respectively 0.12 °CA and 0.05 °CA and 0.05 bar and 0.02 bar respectively for Diesel fuel and HVO.

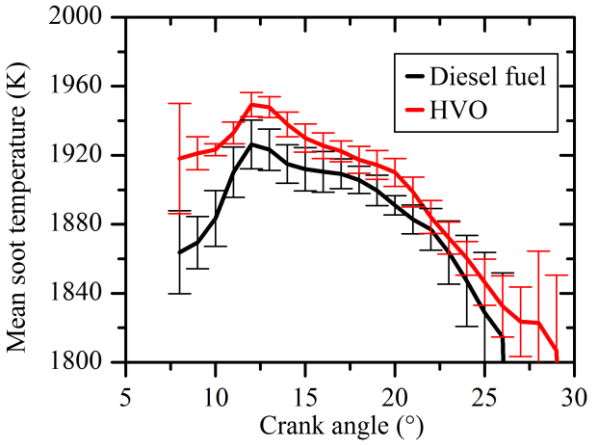


**Figure 8** Mean temperatures of the two fuels and standard deviations between the 10 repetition cycles

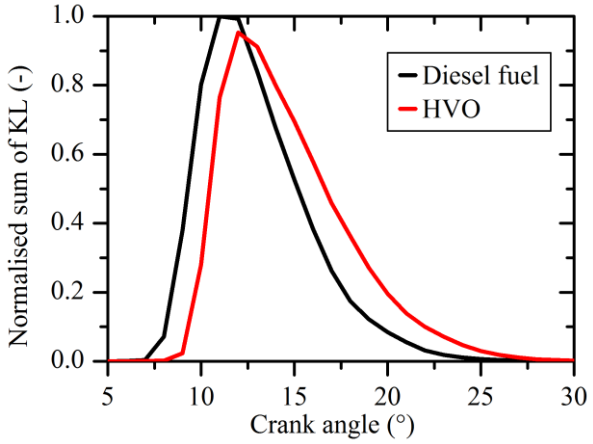


**Figure 9** Normalised sum of the KL-factor

Figure 9 illustrates the averaged over 10 cycles sum of the KL-factors of all pixels normalised to the highest value for Diesel. The peak of the sum of the calculated KL-factors of HVO is slightly smaller than that of the Diesel fuel and is shifted towards a later crank angle position. However the difference in the sum of KL between the fuels is less evident in Figure 9, than in the detected soot areas in Figure 5.This trend indicates generally lower KL values in the case of HVO, about 20 % according to the calculated mean KL-factors showed in Figure 6. The larger soot areas and at the same time lower KL values measured for the HVO indicate larger soot clouds with lesser density, which may be favourable for the oxidation processes, because of the better oxygen availability. HVO has a higher cetane number, but a delayed soot formation, see Figure 9, which may be a result of better air-fuel mixture or a faster oxidation.

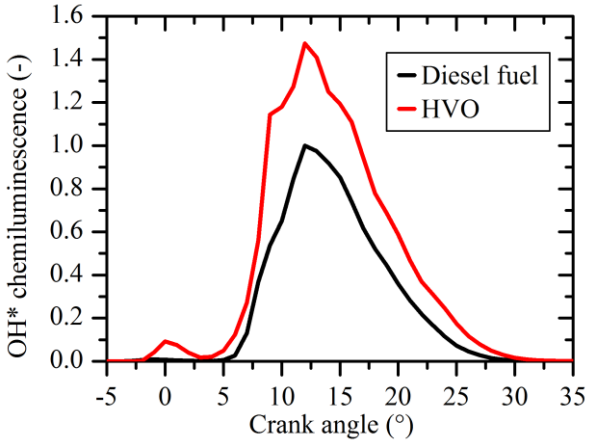


**Figure 10** Normalised average sum of OH* chemiluminesence

The detected intensity of the OH* chemi-luminescence for both fuels is shown in Figure 10. At TDC a small peak marking the combustion of the pilot injection of HVO is noticeable, whereas the measured intensities of the OH radicals for the Diesel fuel are significantly lower, indicating a better burning of HVO.

Moreover considerably stronger OH* chemi-luminescence with up to 50% at its peak could be detected during the combustion of the main injection of HVO as well. There are generally two ways to get the oxygen for the oxidation of the soot from either $O_2$ or OH* radicals. According to [12] OH radicals interact directly with the soot molecules and are required for the oxidation process to take place. OH* radicals are generated in zones with near-stoichiometric conditions where the combustion temperature is highest, which is in agreement with the higher soot temperatures measured for HVO. For high temperature combustions the soot oxidation via OH radicals is dominant method as stated by [13].

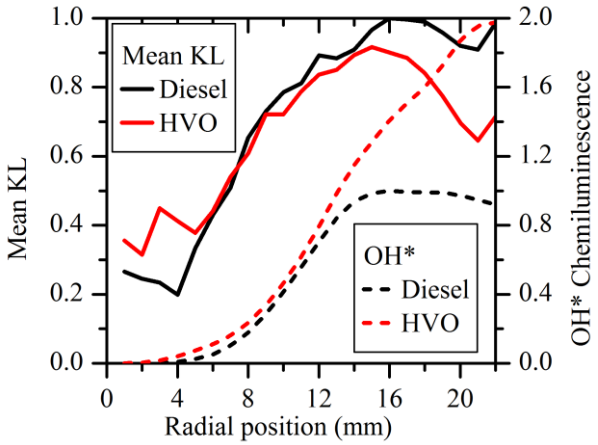


**Figure 11** OH* chemiluminescence and mean KL-factor as function of the radial position in the cylinder

The spray-wall interaction and the region near piston walls in general have a strong impact on soot formation and exhaust emission. Therefore Figure 11 illustrates

the average (5 to 25 °CA after TDC) measured intensities of the OH* radicals and the mean KL-factors for both fuels as a function of the radial position in the cylinder. With increasing proximity to the piston walls higher KL values and thereby denser soot clouds can be observed. However in the region near the piston walls lower mean KL-factors were measured for HVO. Moreover considerably stronger presence of OH* radicals could be detected in this region indicating enhanced oxidation.

**Conclusions**

The burn behaviour and particularly the soot formation and oxidation processes of common Diesel fuel and HVO were investigated in an optically accessible Diesel engine. The combustion analysis of the fuels was performed by simultaneous two-colour imaging as well as detection of OH* chemi-luminescence. The total soot exhaust emissions were also measured using a smoke opacimeter to correlate the optical investigations with engine emissions.

The investigations of the soot luminosity showed nearly 20 % larger soot area for the most part of the combustion, but 50% lower smoke opacity for HVO compared with Diesel and lower mean KL-factors meaning lower in-cylinder soot density for HVO

Since the soot area is larger and the soot particle densities featured by KL are lower in the case of HVO there is an improved oxygen availability. At the same time up to almost 50 % stronger OH* emission could be detected for HVO also indicating superior oxidation characteristics. Evaluating the two-colour images higher and more uniformly distributed soot temperatures with lower cyclic fluctuations could be noticed for HVO. The stronger presence of OH* also supports this trend of higher combustion temperatures in the case HVO and as pointed out by [13] higher temperatures can be favourable for the soot oxidation.

In future works investigations with other alternative fuels of the second generation will be included, where also their atomisation and spray characteristics will be analysed and correlated with the combustion investigations. Moreover in order to extend the understanding of the soot formation and oxidation the temporal soot evolution will be investigated.

**Acknowledgements**

The authors thank the federal state Sachsen-Anhalt financial support of this work in the Framework of the COMO project, and the Institute of Automotive Expertise for providing the opportunity to work on their state-of-the-art single-cylinder test bed.

**References**

1. Schulze, T., *Untersuchung des Einflusses der Spritzlochgeometrie der Einspritzdüse auf die dieselmotorische Gemischbildung und Verbrennung.* "Friedrich List" faculty of Transportation and traffic sciences, Technical University Dresden, 2005. **Dissertation**.
2. Greis, A.E., *Laseroptische Untersuchungen des Verbrennungsprozesses in einem PKW-Dieselmotor.* Faculty of Mechanical Engineering, RWTH Aachen University, 2007. **Dissertation**.
3. Gaydon, A.G., *The Spectroscopy of Flames*. 2 ed. 1974: Chapman and Hall.
4. Hottel, H.C., Broughton, F.P. , *Determination of True Temperature and Total Radiation from Luminous Gas Flames.* Industrial and Engineering Chemistry: Analytical Edition, 1932. **4**(2): p. 166-175.
5. Zhao, H., Ladommatos, N. , *Optical Diagnostics for Soot and Temperature Measurement in Diesel Engines.* Prog. Energy Combust. Sci., 1998. **24**: p. 221-255.
6. Matsuura, K., Suzuki, O., and Kato, A.,, *In-cylinder Optical Investigation of Combustion Behavior on a Fast Injection Rate Diesel Common Rail Injector.* SAE Int. J. Fuels Lubr., 2012. **5**(1): p. 88-97.
7. Zha, K., Yu, X., Florea, R., Jansons, M., *Impact of Biodiesel Blends on In-cylinder Soot Temperature and Concentrations in a Small-Bore Optical Diesel Engine.* SAE Technical Paper, 2012. **2012-01-1311**.
8. Svensson, K.I., Mackrory, Andrew J., Richards, Michael J., Tree, Dale R., *Calibration of an RGB, CCD Camera and Interpretation of its Two-Color Images for KL and Temperature.* SAE Technical Paper, 2005. **2005-01-0648**.
9. Jakob, M., Hülser, T., Janssen, A., Adomeit, P., Pischinger, S., Grünefeld, G., *Simultanious high-speed visualisation of soot luminosity and OH* chemiluminescence of alternative-fuel combustion in a HSDI diesel engine under realistic operating conditions.* Combustion and Flame, 2012. **159**(7): p. 2516-2529.
10. Zannis, T.C., Hountalas, R.G., Papaglannakis, R.G., Levendis, Y.A., *Effect of fuel chemical structure and properties on diesel engine performance and pollutant emissions: review of the results of four European research programs.* SAE Technical Paper, 2008. **2008-01-0838**.
11. Hottenbach, P., Brands, T., Grünefeld, G., Janssen, A., Müther, M., Pischinger, S., *Optical and Thermodynamic Investigations of Reference Fuels for Future Combustion System.* SAE Int. J. Fuels Lubr., 2010. **3**(2): p. 819-838.
12. Joos, F., *Technische Verbrennung*. 2006: Springer-Verlag Berlin Heidelberg.
13. Bolla, M., *Modeling soot formation in Diesel engines using conditional moment closure.* ETH Zürich, 2013. **Dissertation**.